Cheung *et al. Nanoscale Research Letters* (2016) 11:459
DOI 10.1186/s11671-016-1666-4

Nanoscale Research Letters

NANO EXPRESS Open Access

Spin Orbit Coupling Gap and Indirect Gap in Strain-Tuned Topological Insulator-Antimonene

Chi-Ho Cheung[1,2*], Huei-Ru Fuh[2], Ming-Chien Hsu[2], Yeu-Chung Lin[2] and Ching-Ray Chang[2]

Abstract

Recently, searching large-bulk band gap topological insulator (TI) is under intensive study. Through $k \cdot P$ theory and first-principles calculations analysis on antimonene, we find that α-phase antimonene can be tuned to a 2D TI under an in-plane anisotropic strain and the magnitude of direct bulk band gap (SOC gap) depends on the strength of spin-orbit coupling (SOC) which is strain-dependent. As the band inversion of this TI accompanies with an indirect band gap, the TI bulk band gap is the indirect band gap, not the SOC gap. SOC gap can be enhanced by increasing strain, whereas the indirect band gap can be closed by increasing strain, such that large bulk band gap are forbidden. With the $k \cdot P$ theory analysis on antimonene, we know how to avoid such an indirect band gap. In case of indirect band gap avoided, the SOC gap could become the bulk band gap of a TI which can be enhanced by strain. Thus our theoretical analysis can help searching large bulk band gap TI.

Keywords: Topological insulator, Large-bulk band gap

Background

In the past 10 years, topological insulator phase has emerged in condensed matter physics with theoretical predictions and experimental observations of this phase in real materials [1–32]. When a material turns into TI phase, it is insulating in the bulk band and conducting on the surface (or edge in two dimensions). The surface states are protected by time reversal symmetry (TRS) and have spin momentum locking property.

Nowadays, the size of manufactured semiconductors almost reaches atomic scale, so it is important to have a breakthrough development in new device operation mechanisms. A utilization of the spin property of electrons is one of the promising venues. Since TI has TRS protected surface states with spin momentum locking property, it could be applied to spintronic devices.

Due to the soaring prices of rare earth materials, narrow bulk band gaps, and stringent ambient condition requirements, TI materials so far available are not practical for industrial production. Thus, searching new TI material or transforming a normal insulator into a topological one are still issues of immediate interest.

Band inversion is a necessary condition for inducing TI phase. Applying strain is one of the methods to cause a band inversion. If spin-orbit coupling (SOC) is ignored, system usually becomes metallic due to the band crossing caused by the band inversion between the highest valence band (VBM) and the lowest conduction band (CBM). SOC is the key to opening a gap (SOC gap) at such crossing point to keep the systems remaining insulating in bulk and meet another necessary condition of inducing TI phase. Furthermore, if TI phase is induced, and the bulk band gap is large enough, such a TI phase continues to exist at room temperature and has a small finite size effect [33] and may become one of the promising candidates of spintronic devices.

The first-principles calculation results of strained α-phase antimonene shows that strain not only can induce TI phase on antimonene but also can enhance the magnitude of TI's direct bulk band gap (SOC gap), such that the magnitude of the SOC gap no longer depends on the atomic order only. We know the reason of this phenomenon is because the strain can enhance the SOC between VBM and CBM, such that the SOC opens a larger

*Correspondence: f98245017@ntu.edu.tw
[1]Graduate Institute of Applied Physics, National Taiwan University, Taipei 10617, Taiwan
Full list of author information is available at the end of the article

band gap in antimonene. Unfortunately, the band inversion accompany with an indirect band gap; thus, the SOC gap is not the bulk band gap of antimonene. Through $k \cdot P$ theory, we learn that, in an anisotropic system, the band inversion of a TI phase transition will accompany with an indirect band gap if VBM and CBM cannot couple to each other by non-SOC $k \cdot P$ term.

Such a theoretical and numerical analysis makes it clear how the strain tunes the SOC gap of a TI and the cause of the indirect band gap. It can help applying such a mechanism on other materials to achieve the goal of searching large bulk band gap TI among light atoms to meet the requirement of spintronic devices with low prices.

Crystal Structure

Our system is a monolayer puckered honeycomb antimonene, which belongs to space group no. 53-Pmna [34–36], and its crystal structure is shown at Fig. 1.

We have simulated the situations in which antimonene finds itself under an in-plane isotropic compress strain and an in-plane anisotropic strain. The applied strain is defined as $\frac{a-a_0}{a_0} \times 100$ %, where a and a_0 are the lattice constants for the strained and relaxed structures, respectively. During the relaxation, we force the x and y direction lattice constants of the unit cell to remain intact, and every atom is free to move to its equilibrium position. Isotropic or anisotropic strain changes lattice constant and the structure parameters, but the crystal structure symmetry remains the same.

Methods

The first-principles calculations are performed by the Vienna Ab initio Simulation Package (VASP) [37, 38]. We use the generalized gradient approximation (GGA) and the Perdew-Burke-Ernzerhof (PBE) exchange-correlation functional along with the projector-augmented wave potentials for self-consistent total energy calculations and geometry optimization. The critical strain for topological phase transition depends on the band gap of antimonene. In order to avoid underestimating the critical strain, hybrid Heyd-Scuseria-Ernzerhof (HSE)06 method [39] should be used, but as this paper is to give qualitative analysis on SOC gap and indirect band gap of TI instead of quantitative prediction for the critical strain of topological phase transition, therefore (HSE)06 method is not used in our first-principles calculations. The energy convergence criteria for electronic and ionic iterations are set to be 10^{-8} eV. The reciprocal space is meshed at $12 \times 16 \times 1$ using the Gamma-centered grid method. The kinetic energy cutoff for the plane wave basis is 500 eV. In order to simulate a monolayer of antimonene, a unit cell with periodic boundary conditions is used. A vacuum space of 1.2 nm was applied to minimize the interaction between the monolayers.

Results and Discussion

Strained Antimonene Without Considering SOC

In this subsection, we analyze the band curvature of strained antimonene with $k \cdot P$ theory. It is well known that from Schrödinger equation and Bloch wave function, the Hamiltonian for a 2D system can be written in the following form:

$$H_0 = \frac{\hbar^2}{2m_0}\left(k_x^2 + k_y^2\right), \tag{1}$$

$$H_{k\cdot P} = \frac{\hbar^2}{m_0}(k_x P_x + k_y P_y), \tag{2}$$

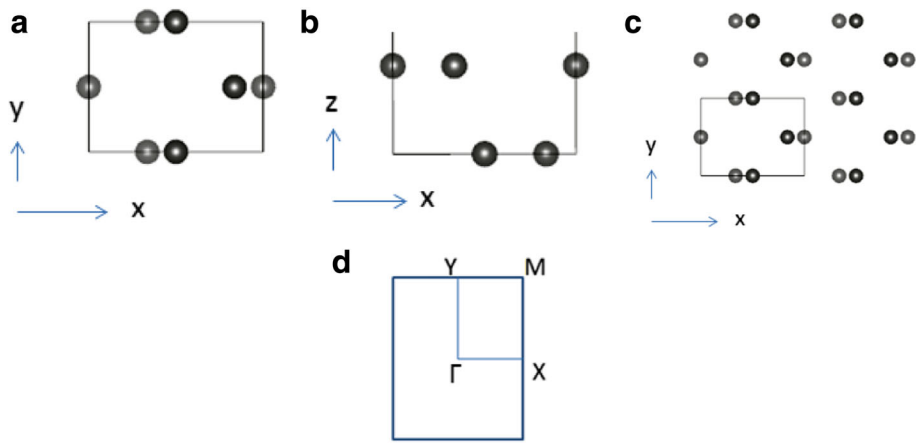

Fig. 1 The crystal structure of monolayer antimonene. **a**, **c** The top views of the monolayer. **b** Side profile view. **d** The first Brillouin zone of the monolayer antimonene. The isotropic or anisotropic strain in this paper change lattice constant and the structure parameters, but the crystal structure symmetry remains intact

$$H_{SO} = \frac{\hbar}{4m_0^2c^2} \nabla V \times \vec{P} \cdot \vec{\sigma}, \tag{3}$$

$$H_{SO,k} = \frac{\hbar}{4m_0^2c^2} \nabla V \times \vec{k} \cdot \vec{\sigma}, \tag{4}$$

where k is the wavenumber, $\hbar$ is the reduced Planck constant, m_0 is the electron rest mass, c is the speed of light, V is the potential, $\vec{P}$ is a momentum operator, σ is Pauli matrix, H_0 is the free electron energy dispersion, $H_{k.P}$ is the non-SOC $k \cdot P$ perturbative terms, H_{SO} is the k-independent SOC perturbative terms and $H_{SO,k}$ is the k-dependent SOC perturbative terms. Since we have not yet considered the SOC, so H_{SO} and $H_{SO,k}$ are ignored in this subsection.

Here, we present a three-band model, in which the first two bands are the second highest and the highest valence bands, and the third one is the lowest conduction band (under zero strain). The band indices of these three bands are 1, 2, and 3, from the lowest to the highest, respectively. Below is the effective Hamiltonian of the three-band model,

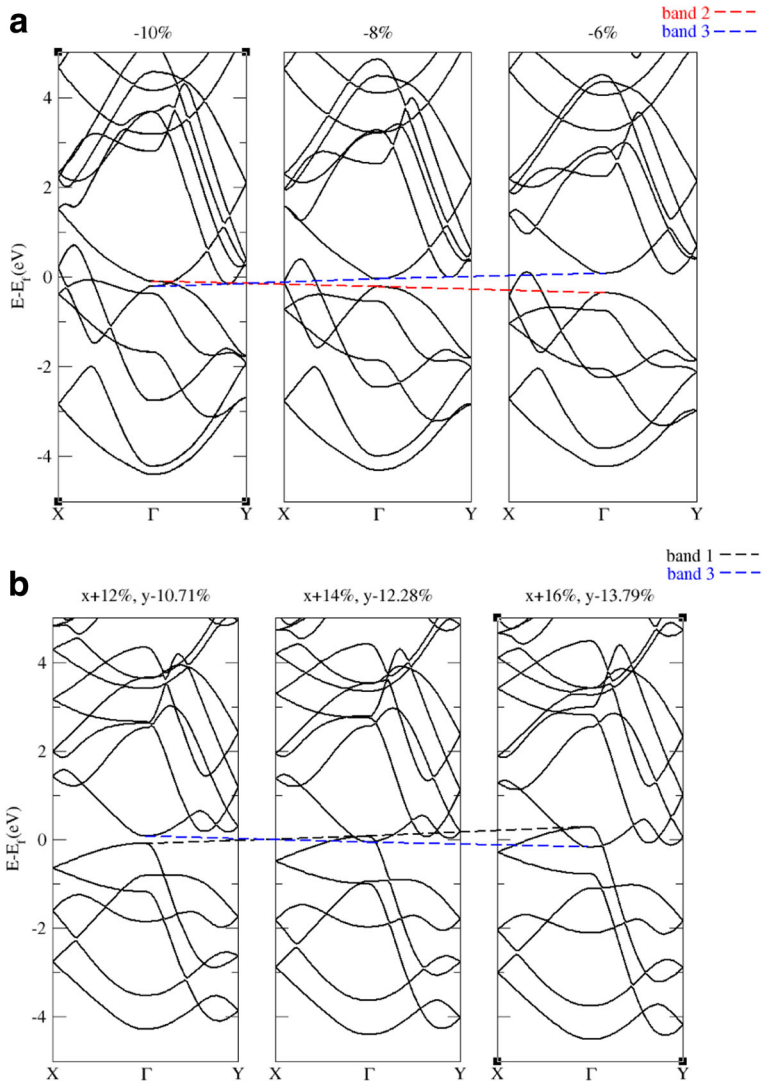

Fig. 2 a Band structures with −6, −8, and − 10 % in-plane isotropic strain. **b** Band structures with different values of in-plane anisotropic strain. *Positive strain* indicates expansion and *negative strain* indicates compression. All energies are referenced to Fermi level. The *dashed lines* are merely a guide for viewing the energy shifts of each band. As band 2 and band 3 are coupled at k_x direction while decoupled at k_y direction, band structure of these two bands become saddle-shaped after band inversion in a way that there is a band crossing point between VBM and CBM in k_y direction. Band 1 and band 3 are decoupled; band inversion does not change the curvature of these two bands; thus, there is a band crossing between VBM and CBM in each k direction. Such band crossing phenomena can be predicted by $k \cdot P$ and group theory

$$H_t = \begin{pmatrix} < u_1|H_t|u_1 > & < u_1|H_t|u_2 > & < u_1|H_t|u_3 > \\ < u_2|H_t|u_1 > & < u_2|H_t|u_2 > & < u_2|H_t|u_3 > \\ < u_3|H_t|u_1 > & < u_3|H_t|u_2 > & < u_3|H_t|u_3 > \end{pmatrix} = \begin{pmatrix} A_{11}k^2 + C_1 & 0 & 0 \\ 0 & A_{22}k^2 + C_2 & A_{23}k_x \\ 0 & A_{23}^* k_x & A_{33}k^2 + C_3 \end{pmatrix}, \quad (5)$$

where $H_t = H_0 + H_{k\cdot P}, u_n$ is the Γ point state wave function of the nth band, A_{nm} is the coefficient of matrix element $< u_n|H_t|u_m >$, n, m = 1, 2, 3, and C_1, C_2, C_3 are the Γ point energy of band 1, 2, 3, respectively.

In Eq. 5, we apply group theory to examine whether or not the matrix element $< u_n|O|u_m >$ of the operator O vanishes. This matrix element can be nonzero only if the irreducible representation (IRR) associated with the operator O is included in the direct sum decomposition of the direct product of the two IRRs of the basis functions [40–42]. Consequently, band 1 does not couple to band 2 or band 3, but band 2 and band 3 are coupled in x direction.

It should be noted that either isotropic or anisotropic strain, which mentioned in "Crystal Structure" section, does not change the symmetry of antimonene, so the form of the effective Hamiltonian does not change either [43]. Thus, we can use the symmetry discussion of space group No.53-*Pmna* to simplify the effective Hamiltonian.

Applying the Löwdin partition to the first order approximation, the energy dispersion relation for each band is

$$E_{nk} \approx H_{nn} + \sum_{\alpha \neq n} \frac{H_{n\alpha}H_{\alpha n}}{E - H_{\alpha\alpha}}, \quad (6)$$

where E_{nk} is the energy of band n with a wavenumber $k, E - H_{\alpha\alpha}$ is the energy difference between band n and band α at Γ point. Finally, $H_{nn}, H_{n\alpha}$, and $H_{\alpha n}$ are the matrix elements in Eq. 5 with $n, \alpha = 1, 2, 3$.

Equation 6 implies that if strain induces band inversion between VBM and CBM, then the second term of the dispersion relation of VBM and CBM changes sign as the energy gap between these two bands changes sign. Consequently, if only k_x term or only k_y term exists in the coupling term of the $k \cdot P$ Hamiltonian of these two bands, the band curvature of these two bands in one of the directions changes sign after the band inversion while the curvature in another direction remains the same and the band structure of these two bands become saddle shaped, such that there will be a band crossing point between VBM and CBM in one of the k directions, as shown in Fig. 2a. If the coupling term of the $k \cdot P$ Hamiltonian of these two bands is zero, the curvature of these two bands remains the same, thus there will be a band crossing point between VBM and CBM in each k direction, as shown in Fig. 2b.

Crossing in one of the k directions or in both k_x and k_y directions is critical to an indirect band gap of the system which will be further discussed at the end of the later subsection.

SOC Gap and Indirect Band Gap of a Topological Insulator

In this subsection, at first, we show how SOC can open a band gap at crossing point. Then, we give the evidence proving the existence of TI phase in antimonene and show how the SOC gap depends on strain. Finally, we discuss how to avoid an indirect band gap that accompanies with the band inversion of a TI.

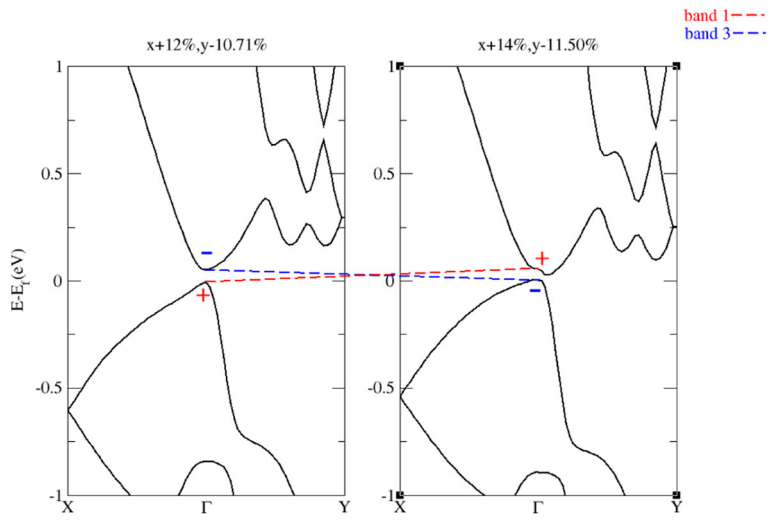

Fig. 3 Band structures before (*left*) and after (*right*) the band inversion. *Positive strain* indicates expansion and *negative strain* indicates compression. All energies are referenced to Fermi level. The *dashed lines* are merely a guide for viewing the energy shifts of each band. The *signs* (+,—) (associate with band 1, 3) indicate the parities of the wavefunctions of Γ point states. The band structures show that, when considering SOC, antimonene can remain in insulator phase after the band inversion

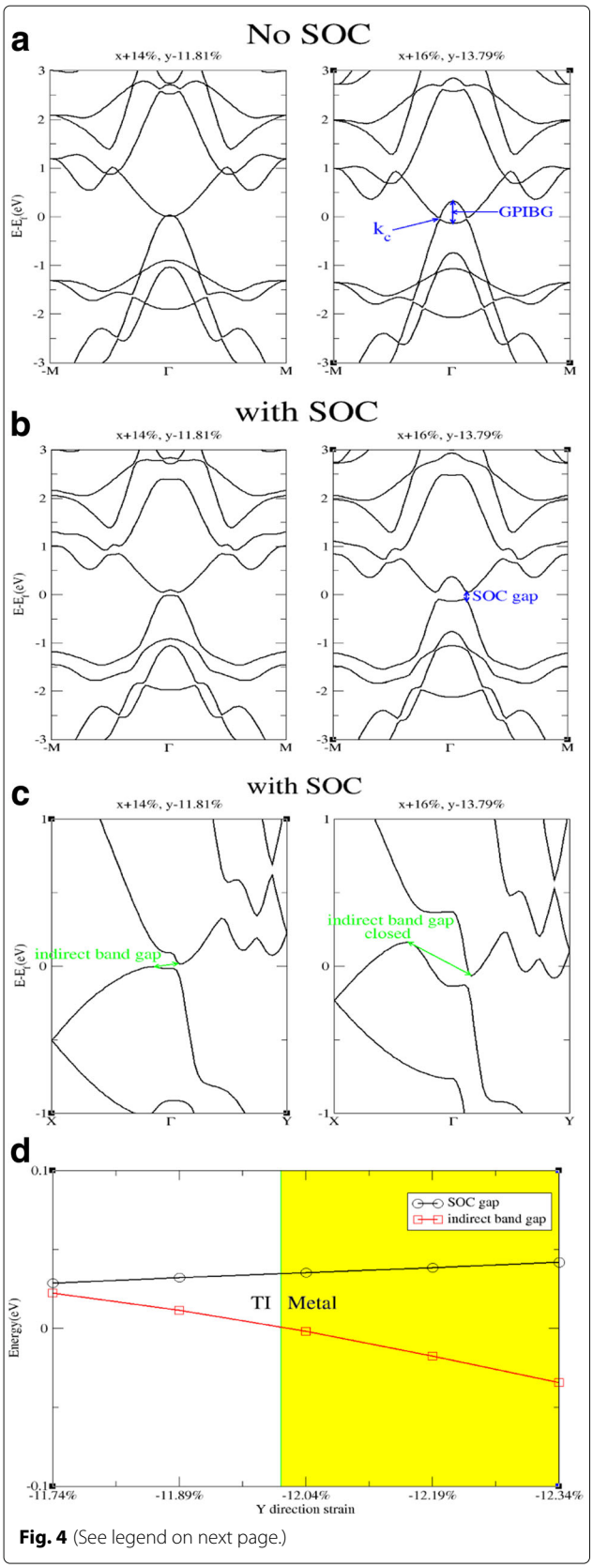

Fig. 4 (See legend on next page.)

(See figure on previous page.)
Fig. 4 k_c is the crossing point of VBM and CBM. The band structures in **a** and **b** show that a larger strain can induce a larger Γ point inversed band gap (GPIBG). The magnitude of k_c will be increased as GPIBG becomes larger. Since the strength of SOC $|A|$ increases as k does, thus, the magnitude of SOC gap increases as k_c does. Therefore, the SOC gap can be enhanced by strain. **c** The band structures of strained antimonene with the other high symmetry points. Due to the anisotropic property of α-phase antimonene, the x direction crossing point locates at a higher energy level than that of in y direction and causes an indirect bulk band gap. While the strain increases, the SOC gap is increased, but the energy difference between x direction crossing point and y direction crossing point is increased too. Consequently, the bulk band gap will close again when the strain becomes too large. **d** The magnitude of the SOC gap in k_y direction and the indirect bulk band gap of antimonene against different values of y direction strain (x direction strain is +14 %); negative indirect bulk band gaps indicate that the indirect bulk band gap of antimonene is closed and the system turns into a metal

The last subsection has already shown that strain can induce band inversion at Γ point and causes a band crossing point in k_x or k_y direct.

Treating SOC as a perturbative term, and considering a two-band modeling Hamiltonian at the band crossing point:

$$H = \begin{pmatrix} E_{k\cdot P} & A \\ A^* & E''_{k\cdot P} \end{pmatrix}, \tag{7}$$

where $E_{k\cdot P}$ and $E''_{k\cdot P}$ are the bands' energy without considering SOC, and A is the SOC term. At the crossing point, these two bands are degenerated; thus, $E_{k\cdot P} = E''_{k\cdot P}$. The energy eigenvalues of Eq. 7 are $E_{k\cdot P} \pm |A|$, which means these two bands open a gap at the crossing point, and the magnitude of the gap is $2|A|$ being proportional to the strength of SOC.

Since the band gap is opened by SOC, strained antimonene can be insulating in bulk after the band inversion (as shown in Fig. 3). As strained antimonene has central inversion symmetry and the band inversion at Γ point exchanges the opposite parity of VBM and CBM, thus, strained antimonene may have topological insulator phase.

It is well known that the nature of topology phase of a system can be examined by its parity product of all the time reversal invariant (TRI) momentum points. Therefore, we calculate the Z_2 index of the system to confirm the topological insulator phase [14].

The Z_2 index ν can be calculated by the following equation,

$$(-1)^{\nu} = \prod_i \Theta_i, \tag{8}$$

where

$$\Theta_i = \prod_{n=1}^{N} \vartheta_{2n}(\Gamma_i), \tag{9}$$

in which 2N is total number of occupied bands, and $\vartheta_{2n}(\Gamma_i)$ is the parity eigenvalue of the 2n-th occupied band at the time reversal invariant momentum Γ_i. Our first-principles calculations show that the Z_2 index is zero before the band inversion. Just after the band inversion, Z_2 invariant changes from 0 to 1, meaning that the system is changed to be a TI.

Without considering SOC, strained antimonene has a band crossing between VBM and CBM at some $k = k_c$ point after the band inversion and such a crossing point can be located at a larger k point while the Γ point inversed band gap (GPIBG) is larger (as shown in Fig. 4). Furthermore, since the SOC term has k-dependent part (as shown in Eq. 4), the strength of SOC $|A|$ is k-dependent. While considering SOC which opens a band gap at the crossing point, the magnitude of the SOC gap depends on the strength of SOC which increases as the magnitude of k_c increases. Since the Γ point inversed band gap (GPIBG) can be tuned by strain, the SOC gap at k_c can simultaneously be enhanced by strain.

Unfortunately, the magnitude of SOC gap is not the value of bulk band gap of antimonene. Due to the anisotropic property of α-phase antimonene, the x direction crossing point locates at a higher energy level than that in y direction and causes an indirect bulk band gap. When the strain increases, the SOC gap is increased, but the energy difference between x direction crossing point and y direction crossing point is increased too. Consequently, the bulk band gap will eventually close again when the strain becomes too large (as shown in Fig. 4c, d).

There are two ways to avoid such an indirect band gap closing. One is applying strain on a system of more isotropic. The other is applying strain on an anisotropic system whose VBM and CBM are coupled to each other in one of the k directions by non-SOC $k \cdot P$ term. One of the examples is applying in-plane isotropic strain on antimonene. In-plane isotropic strain can cause a band inversion between band 2 and band 3. As shown in Eq. 5, band 2 and band 3 are coupled in k_x direction while decoupled in k_y direction. Thus, there are only one crossing point between band 2 and band 3 after the band inversion. Therefore, the band inversion does not cause an indirect band gap around the Γ point (as shown in Fig. 5). Even though the in-plane isotropic strain turns antimonene to be a metal before causing the band inversion between band 2 and band 3 (as shown in Fig. 2a) and consequently TI phase is forbidden in this case, there are other cases that, in other materials or with other band inversion mechanisms, transition to metal phase can be avoided. An example in reference [44] shows that electric field can induce a band inversion between VBM and CBM as the VBM and CBM are coupled to each other in one of the k directions by non-SOC $k \cdot P$ term, an indirect band gap accompanying with the band inversion is avoided even though the system has an anisotropic property. This example implies that transition to metal phase can be avoided in some cases.

Based on this band analysis of antimonene, we suggest the mechanism of inducing strain-enhanced SOC gap should apply to systems of more isotropic or to other anisotropic systems whose VBM and CBM are coupled to each other in one of the k directions by non-SOC $k \cdot P$ term for achieving the goal of searching large bulk band gap TI.

There are some reports that some large bulk band gap TI systems are stable under strain and can be candidate materials for spintronics device [1, 3, 8]. Even though antimonene is not stable under large strain, the methodology of finding lager band gap spintronics device is still valid; a further study of finding those large band gap TI can be accelerated with the help of our proposed band analysis.

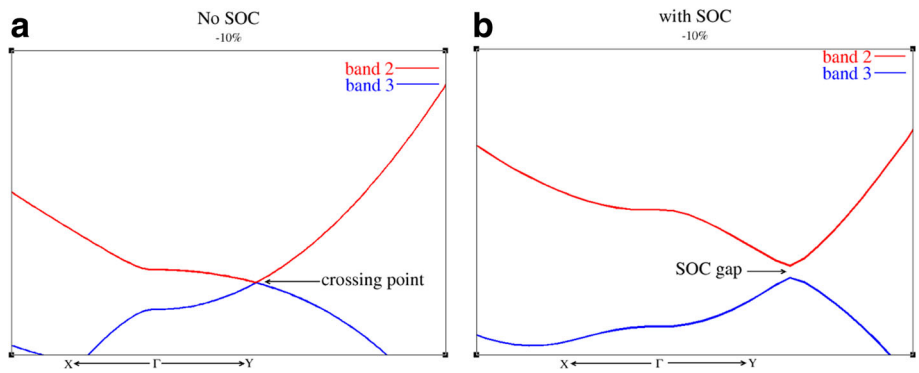

Fig. 5 The band structure of strained antimonene. **a** Without SOC. **b** With SOC. The in-plane isotropic strain causes a band inversion between band 2 and band 3. Since band 2 and band 3 are decoupled in k_y direction but coupled in k_x direction by non-SOC $k \cdot P$ term, band inversion between CBM and VBM cause only one crossing point. After considering SOC, a band gap open at the crossing point. Because there are only one crossing point, this band inversion does not accompany with an indirect band gap around the Γ point which is different with the band inversion between band 1 and band 3 (as shown in Fig. 4c)

Conclusions

In this paper, we analyze antimonene with $k \cdot P$ theory and find that without considering SOC, strain-induced Γ point band inversion would cause band crossing between VBM and CBM and the system simply turns into metallic state. With SOC included, band gap opens at the crossing point in a way that antimonene remains insulating after the band inversion. Then, we use Z_2 invariant to prove that while strained antimonene remains in insulator phase after the band inversion, antimonene has a topological non-trivial phase.

Furthermore, because strain can enhance the spin-orbit coupling between VBM and CBM at the crossing point, the SOC gap increases as the strain does. With such a mechanism, the magnitude of the SOC gap no longer depends on the atomic order only. Thus, searching large bulk band gap TI among light atoms becomes possible, though the SOC gap is not always the bulk band gap of a TI.

The $k \cdot P$ theory indicates that, in an anisotropic system, the band inversion of a TI phase transition will accompany with an indirect band gap if VBM and CBM cannot couple to each other by non-SOC $k \cdot P$ term. The magnitude of such an indirect band gap decreases as the strain increases. With the indirect band gap, the SOC gap cannot be the bulk band gap. Therefore, the indirect band gap should be avoided. Inducing strain-enhanced SOC gap should be promoted to more isotropic systems or to other anisotropic systems whose VBM and CBM are coupled to each other in one of the k directions by non-SOC $k \cdot P$ term.

Acknowledgments

This work studied was supported by the Ministry of Science and Technology of Taiwan under Grant No. MOST 104-2112-M-002-007-MY3 and Ministry of Economic Affairs of Taiwan under Grant No. 102-EC-17-A-01-S1-219 and technically supported by Computer and Information Networking Center of National Taiwan University.

Authors' contributions

CHC carried out much of the analytical and numerical studies and wrote the manuscript. HRF contributed mainly to the numerical part. MCH contributed mainly to the analytic part. YCL and CRC supervised the project. All authors read and approved the final manuscript.

Competing interests

The authors declare that they have no competing interests.

Author details

[1]Graduate Institute of Applied Physics, National Taiwan University, Taipei 10617, Taiwan. [2]Department of Physics, National Taiwan University, Taipei 10617, Taiwan.

Received: 2 May 2016 Accepted: 29 September 2016
Published online: 18 October 2016

References

1. Wang YP, Ji WX, Zhang CW, Li P, Li F, Ren MJ, Chen XL, Yuan M, Wang PJ (2016) Controllable band structure and topological phase transition in two-dimensional hydrogenated arsenene. Sci Rep 6:20342
2. Wang YP, Zhang CW, Ji WX, Zhang RW, Li P, Wang PJ, Ren MJ, Chen XL, Yuan M (2016) Tunable quantum spin hall effect via strain in two-dimensional arsenene monolayer. J Phys D: Appl Phys 49:055305
3. Zhang RW, Zhang CW, Ji WX, Li SS, Yan SS, Li P, Wang PJ (2016) Functionalized thallium antimony films as excellent candidates for large-gap quantum spin hall insulator. Sci Rep 6:21351
4. Yan B, Jansen M, Felser C (2013) A large-energy-gap oxide topological insulator based on the superconductor $BaBiO_3$. Nat Phys 9:709
5. Shen L, Zeng M, Lu Y, Yang M, Feng YP (2013) Simultaneous magnetic and charge doping of topological insulators with carbon. Phys Rev Lett 111:236803
6. Kane CL, Mele EJ (2005a) Quantum spin hall effect in raphene. Phys Rev Lett 95:226801
7. Kane CL, Mele EJ (2005b) Z_2 topological order and the quantum spin hall effect. Phys Rev Lett 95:146802
8. Zhao M, Zhang X, Li L (2015) Strain-driven band inversion and topological aspects in Antimonene. Sci Rep 5:16108
9. Chuang FC, Yao LZ, Huang ZQ, Liu YT, Hsu CH, Das T, Lin H, Bansil A (2014) Prediction of large-gap two-dimensional topological insulators consisting of bilayers of group III elements with Bi. Nano Lett 14:2505–2508
10. Winterfeld L, Agapito LA, Lin J, Kioussis N, Blaha P, Chen YP (2013) Strain-induced topological insulator phase transition in HgSe. Phys Rev B 87:075143
11. Moore JE, Balents L (2007) Topological invariants of time-reversal-invariant band structures. Phys Rev B 75:121306(R)
12. Roy R (2009) Topological phases and the quantum spin Hall effect in three dimensions. Phys Rev B 79:195322
13. Bernevig BA, Hughes TL, Zhang SC (2006) Quantum spin hall effect and topological phase transition in HgTe quantum wells. Science 314:1757
14. Fu L, Kane CL (2007) Topological insulators with inversion symmetry. Phys Rev B 76:045302
15. König M, Wiedmann S, Brne C, Roth A, Buhmann H, Molenkamp LW, Qi XL, Zhang SC (2007) Quantum spin hall insulator state in HgTe quantum wells. Science 318:766
16. Hsieh D, Qian D, Wray L, Xia Y, Hor YS, Cava RJ, Hasan MZ (2008) A topological Dirac insulator in a quantum spin Hall phase. Nature 452:970
17. Xia Y, Qian D, Hsieh D, Wray L, Pal A, Lin H, Bansil A, Grauer D, Hor YS, Cava RJ, Hasan MZ (2009) Observation of a large-gap topological-insulator class with a single Dirac cone on the surface. Nat Phys 5:398
18. Zhang H, Liu CX, Qi XL, Dai X, Fang Z, Zhang SC (2009) Topological insulators in Bi_2Se_3, Bi_2Te_3 and Sb_2Te_3 with a single Dirac cone on the surface. Nat Phys 5:438
19. Murakami S (2011) Quantum spin Hall systems and topological insulators. New J Phys 13:105007
20. Zhang W, Yu R, Zhang H-J, Dai X, Fang Z (2010) First-principles studies of the three-dimensional strong topological insulators Bi_2Te_3, Bi_2Se_3 and Sb_2Te_3. New J Phys 12:065013
21. Prodan E (2010) Non-commutative tools for topological insulators. New J Phys 12:065003
22. Lin H, Das T, Wray LA, Xu S-Y, Hasan MZ, Bansil A (2011) An isolated Dirac cone on the surface of ternary tetradymite-like topological insulators. New J Phys 13:095005
23. Hsieh D, Wray L, Qian D, Xia Y, Dil JH, Meier F, Patthey L, Osterwalder J, Bihlmayer G, Hor YS, Cava RJ, Hasan MZ (2010) Direct observation of spin-polarized surface states in the parent compound of a topological insulator using spin- and angle-resolved photoemission spectroscopy in a Mott-polarimetry mode. New J Phys 12:125001
24. Lin S-Y, Chen M, Yang X-B, Zhao Y-J, Wu S-C, Felser C, Yan B (2015) Theoretical search for half-Heusler topological insulators. Phys Rev B 91:094107
25. Jungfleisch MB, Zhang W, Jiang W, Hoffmann A (2015) New Pathways Towards Efficient Metallic Spin Hall Spintronics. SPIN 05:1530005
26. Lee B-R, Chang C-R, Klik I (2014) Spin transport in multiply connected fractal conductors. SPIN 04:1450007
27. Imura KI, Mao S, Yamakage A, Kuramoto Y (2011) Flat edge modes of graphene and of Z_2 topological insulator. Nanoscale Res Lett 6:358. doi:10.1186/1556-276X-6-358
28. Efimkin DK, Lozovik YE, Sokolik AA (2012) Collective excitations on a surface of topological insulator. Nanoscale Res Lett 7:163. doi:10.1186/1556-276X-7-163
29. Bai C, Yang Y (2014) Gate-tuned Josephson effect on the surface of a topological insulator. Nanoscale Res Lett:9515. doi:10.1186/1556-276X-9-515

30. Cao T, Wang S (2013) Topological insulator metamaterials with tunable negative refractive index in the optical region. Nanoscale Res Lett 8:526. doi:10.1186/1556-276X-8-526
31. Bai C, Yang Y (2014) Gate-tuned Josephson effect on the surface of a topological insulator. Nanoscale Res Lett 9:515. doi:10.1186/1556-276X-9-515
32. Lee J-S, Klik I, Chang C-R (2015) Magnetization reversal in a double-walled infinite nanotube. SPIN 05:1550005
33. Hsu MC, Lin YC, Chang CR (2015) Finite size effect of nondegenerate edge states in annulus topological insulators. J Appl Phys 118:043909
34. Ribeiro-Soares J, Almeida RM, Cançado LG, Dresselhaus MS, Jorio A (2015) Group theory for structural analysis and lattice vibrations in phosphorene systems. Phys Rev B 91:205421
35. Kamal C, Ezawa M (2015) Arsenene: Two-dimensional buckled and puckered honeycomb arsenic systems. Phys Rev B 91:085423
36. Lew Yan Voon LC, Lopez-Bezanilla A, Wang J, Zhang Y, Willatzen M (2015) Effective Hamiltonians for phosphorene and silicone. New J Phys 17:025004
37. Kresse G, Furthmüller J (1996) Efficient iterative schemes for ab initio total-energy calculations using a plane-wave basis set. Phys Rev B 54:11169
38. Kresse G, Furthmüller J (1996) Efficiency of ab-initio total energy calculations for metals and semiconductors using a plane-wave basis set. Comput Mater Sci 6:15
39. Paier J, Marsman M, Hummer K, Kresse G, Gerber IC, Ángyán JG (2006) Erratum: "Screened hybrid density functionals applied to solids". J Chem Phys 124:154709
40. Dresselhaus MS (2002) Applications of group theory to the physics of solids. http://web.mit.edu/course/6/6.734j/www/group-full02.pdf
41. Li P, Appelbaum I (2014) Electrons and holes in phosphorene. Phys Rev B 90:115439
42. GALERIU C (2005) $\boldsymbol{k}\cdot\boldsymbol{p}$ Theory of semiconductor nanostructures. https://web.wpi.edu/Pubs/ETD/Available/etd-120905-095359/unrestricted/cgaleriu.pdf
43. Bulutay C (2006) Semiconductor electronic structure and optical processes lecture 8. http://www.fen.bilkent.edu.tr/~bulutay/573/notes/ders_8.pdf
44. Liu Q, Zhang X, Abdalla LB, Fazzio A, Zunger A (2015) Switching a Normal Insulator into a Topological Insulator via Electric Field with Application to Phosphorene. Nano Lett 15:1222–1228